Transition From Weak to Strong Energetic Ion Transport in Burning Plasmas

F. Zonca 1), S. Briguglio 1), L. Chen 2), G. Fogaccia 1), G. Vlad 1)

1) ENEA C. R. Frascati, C.P. 65, 00044 Frascati, Rome, Italy
2) Department of Physics and Astronomy, University of California, Irvine, CA 92717-4575

e-mail contact of main author: fulvio.zonca@frascati.enea.it

Abstract. The change in non-linear EPM dynamics that accompanies the transition from weak to strong energetic ion transport is discussed in the present work. It is demonstrated that the non-linear threshold in fast ion energy density for the onset of strong convective transport occurring in avalanches is close to the linear EPM excitation threshold. This phenomenology is strictly related with the resonant character of the modes, which tend to be radially localized where the drive is strongest. After the convective loss phase, during which non-linear EPM mode structure is displaced outwards, fast ion transport continues due to diffusive processes. Theoretical analyses, presented here, are the basis for consistency analyses of operation scenarios in proposed burning plasma experiments. Comparisons between theoretical predictions and both simulation and experimental results are also briefly discussed.

1. Introduction and Background

A burning plasma is a self-organized system, where collective effects associated with fast ions (MeV energies) and charged fusion products (from now on referred to as fast or energetic ions) may alter their confinement properties and even jeopardize the achievement of ignition. Simulation results indicate that, above threshold for the onset of resonant Energetic Particle Modes (EPM) [1], strong fast ion transport occurs in *avalanches* [2] (see Fig. 1). Such strong transport events occur on time scales of a few inverse linear growth rates (generally, $100 \div 200$ Alfvén times) and have a ballistic character [3] that basically differentiates them from the diffusive and local nature of weak transport. Meanwhile, numerical simulations have demonstrated that Alfvén Cascades in JET [4] are consistent with both weak as well as strong fast ion transport [5]. Recently, experimental observations on the JT-60U tokamak have also confirmed macroscopic and rapid (in the sense discussed above) energetic particle radial redistributions in connection with the so called Abrupt Large amplitude Events (ALE) [6]. Therefore, it is crucial to theoretically assess the potential impact of fusion product avalanches on burning plasma operation in the perspective of direct comparisons with experimental evidence.

The change in non-linear EPM dynamics that accompanies the transition from weak to strong energetic ion transport is discussed in the present work. It is demonstrated that the non-linear threshold in fast ion energy density for the onset of avalanches is close to the linear EPM excitation threshold. This phenomenology is strictly related with the resonant character of the modes, which tend to be radially localized where the drive is strongest [7, 8]. When the non-linear threshold is exceeded, the EPM envelope propagates radially because of two reasons: the radial dispersiveness of the mode and the rapid redistribution of the energetic particle source. These two effects can be viewed as manifestation of linear and, respectively, non-linear EPM radial group velocities. As it propagates, the EPM radial envelope is convectively amplified

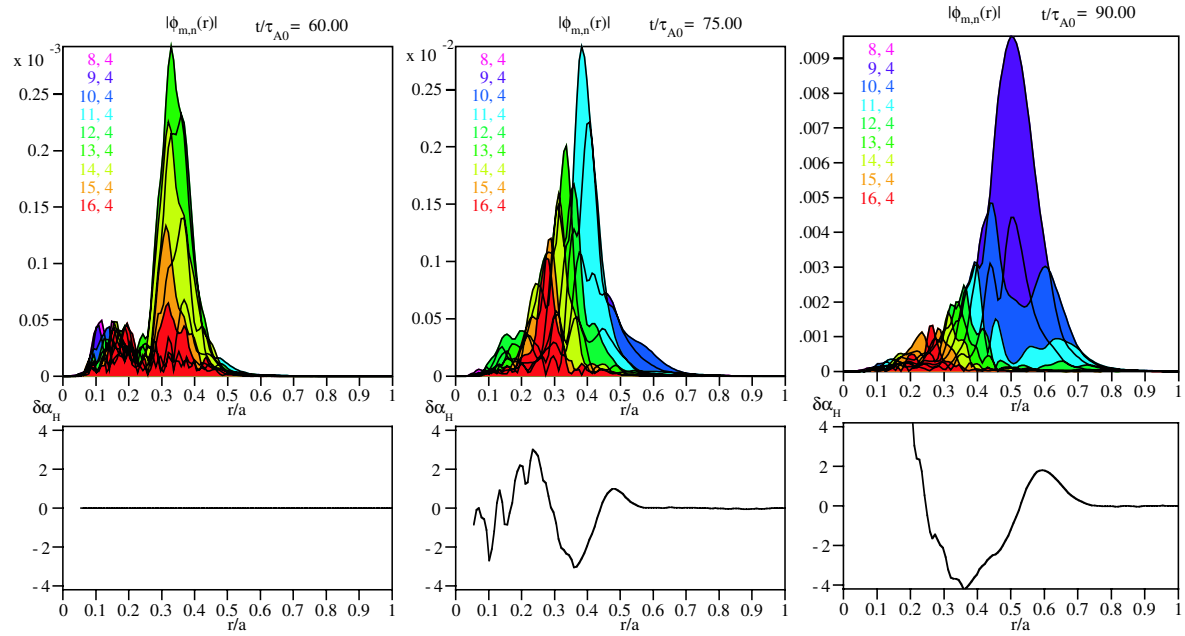

FIG. 1. Time evolution of the EPM radial structure, decomposed in poloidal Fourier harmonics. Here $\tau_{A0} = R_0/v_{A0}$*, with* R_0 *the tokamak major radius and* v_{A0} *the on axis Alfvén speed. The toroidal mode number is* $n = 4$*.* $\delta\alpha_H$ *is the nonlinear modification of the fast ion* $\alpha_H = -R_0 q^2 (d\beta_H/dr)$ *[2].*

due to resonant wave-particle interactions, which are responsible for the secular motion of the unstable front as well and, ultimately, of the avalanching process [9]. After the convective loss phase, during which non-linear EPM mode structure is displaced outwards, fast ion transport continues due to diffusive processes [10, 11].

Our analysis refers to the nonlinear dynamic evolution of a single-n, *i.e.* a single toroidal mode number, coherent shear Alfvén (s.A.) wave, strongly driven in the presence of an isotropic fusion alpha particle population. For the sake of simplicity, we consider a low-β and large aspect ratio tokamak plasma with circular magnetic surfaces. Thus, the ratio of thermal to magnetic energy densities, $\beta = 8\pi P/B_0^2 \ll 1$, $B = B_0 R_0/R$ and the torus minor/major radii are such that $a/R_0 \ll 1$. Meanwhile, we can consider a simple (s, α) model equilibrium, with s the magnetic shear and $\alpha = -R_0 q^2 (d\beta/dr)$, and assume a straight magnetic field line toroidal coordinate system (r, θ, ϕ), with $q(r) = (\mathbf{B} \cdot \nabla\phi / \mathbf{B} \cdot \nabla\theta)$ the safety factor.

The nonlinear dynamics of a single-n coherent s.A. wave is affected via both local and global phenomena. In the first category, the idea of mode saturation via wave-particle trapping [12, 13] has been successfully applied to explain pitchfork splitting of Toroidal Alfvén Eigenmode spectral lines [14]. However, other physical mechanisms can be important, depending on the parameter regimes, as Compton scattering off the thermal ions [15] and mode-mode couplings generating a nonlinear frequency shift which may enhance the interaction with the Alfvén continuous spectrum [16, 17]. All these phenomena are local in the sense they either locally distort the fast ion distribution function because of quasi-linear wave-particle interactions [12, 13], or locally enhance the mode damping either via nonlinear wave-particle [15] or wave-wave interactions [16, 17]. For such a reason, the radial mode structure providing the envelope of the poloidal Fourier harmonics that compose the wave field – see Eq. (5) below – never enters in all these treatments.

Intuitively speaking, the relevance of local phenomena in the nonlinear dynamics of a single-n coherent s.A. wave near marginal stability [18] is readily understood. However, for a resonant mode like the EPM, which is localized where the drive is strongest [7, 8], global readjustments in the energetic particle drive is expected to be important as well. In the following, we will determine under what conditions global phenomena are relevant for EPM nonlinear dynamics and show that these become important right above the linear excitation threshold for the mode. Accounting for local and global phenomena on the same footing is extremely complex and, in this respect, numerical simulations appear to be the optimal tool for such analyses [10, 11]. Hereafter, we neglect local phenomena and consider only global nonlinear EPM dynamics. Our findings will be checked for consistency *a posteriori*.

In the presence of global equilibrium profile changes, the nonlinear dynamics of a single-n coherent EPM can be affected by both $\mathbf{E}\times\mathbf{B}$ shearing due to spontaneously generated zonal flows as well as by nonlinear distortions of the energetic ion source. Of these two processes, the latter is dominant for $(\alpha_H/\beta_i)(T_i/T_H) \gg \epsilon^{3/2}$ [19], where $\alpha_H = -R_0 q^2 (d\beta_H/dr)$, T_H is the fast ion thermal energy, $\epsilon = r/R_0$, r is the radial position where the EPM is localized, and β_i and T_i are the thermal ion β and temperature. This condition is typically satisfied for a resonantly excited EPM. Thus, in the following, we concentrate on the fast ion source nonlinear distortions. More specifically, we analyze these phenomena in the early nonlinear phase, when avalanching occurs [2, 20]. In the late nonlinear phase, besides the fast ion diffusion in the saturated field, radial fragmentation of the coherent EPM eddies can be spontaneously driven by modulational instability of the mode radial envelope due to radial modulations in the energetic particle source. This aspect is analyzed in Ref. [19].

2. Theoretical Analyses

The theoretical framework of our analysis is that of Refs. [9, 19]; *i.e.* we decompose the fluctuating particle distribution function into adiabatic and non-adiabatic responses as [21]

$$\delta F_k = \frac{e}{m}\delta\phi_k \frac{\partial}{\partial v^2/2} F_0 + \sum_{\mathbf{k}_\perp} \exp\left(-\mathrm{i}\mathbf{k}_\perp\cdot\mathbf{v}\times\mathbf{b}/\omega_c\right)\overline{\delta H}_k \quad , \tag{1}$$

where notation is standard and the subscripts H for the energetic ions have been dropped unless needed to avoid confusion. The non-adiabatic response of the particle distribution function, $\overline{\delta H}_k$, is obtained from the NL gyrokinetic equation [21]:

$$\begin{aligned}
&\left(\partial_t + v_\parallel\partial_\ell + \mathrm{i}\omega_d\right)_k \overline{\delta H}_k = \mathrm{i}\frac{e}{m} Q F_0 J_0(\gamma)\delta L_k - \frac{c}{B}\mathbf{b}\cdot\left(\mathbf{k}''_\perp\times\mathbf{k}'_\perp\right) J_0(\gamma')\delta L_{k'}\overline{\delta H}_{k''} \quad , \\
&Q F_0 = \omega_k \frac{\partial F_0}{\partial v^2/2} + \mathbf{k}\cdot\frac{\hat{\mathbf{b}}\times\nabla}{\omega_c} F_0 \quad , \quad \delta L_k = \delta\phi_k - \frac{v_\parallel}{c}\delta A_{\parallel k} \quad ,
\end{aligned} \tag{2}$$

where $\delta\phi_k$ and $\delta A_{\parallel k}$ are the scalar and parallel vector potentials. The present approach is based on treating hot particle distribution consisting of a background one plus a perturbation on a meso time and space scales: thus the background distribution is frozen in time. To solve Eq. (2) for the nonlinear modification of the equilibrium fast particle distribution function in the presence of a coherent EPM, we adopt the procedure of Ref. [22]. Thus, indicating with $\overline{\delta H}_z$ the $(m=0, n=0)$ (*zonal*) energetic ion response, we have

$$\overline{\delta H}_z = \exp\left(-iQ_z\right) H_z \quad , \qquad \mathbf{B}\cdot\nabla H_z = 0 \quad , \qquad Q_z = \frac{q}{(r/R_0)} k_z \frac{v_\parallel}{\omega_c} \quad , \tag{3}$$

where $k_z = (-i\partial_r)$ is the radial wave vector of nonlinear equilibrium profile changes. This is then reduced to a "quasilinear" evolution equation for the meso-scale H_z

$$\frac{\partial}{\partial t} H_z = \sum_{\mathbf{k}_z = \mathbf{k}' + \mathbf{k}''} i \frac{c}{B_0} k'_\theta \frac{\partial}{\partial r} \overline{\left[e^{iQ_z} J_0(\gamma') \delta L_{k'} \overline{\delta H}_{k''} \right]} \quad , \tag{4}$$

with $k'_\phi = -k''_\phi$, $k'_\theta = -k''_\theta$ and $\overline{(...)} = \int (d\ell / v_\parallel) \, (...) \, / \int (d\ell / v_\parallel)$, ℓ being the arc length along $\mathbf{B}$ [22]. In order to make further analytic progress and discuss the EPM nonlinear dynamic evolution, we consider a simple case in which the dominant wave-particle interactions are described via the precession resonance (see, *e.g.* Ref. [11]) and assume that trapped particles move with an harmonic motion about the torus midplane, *i.e.* they behave as deeply trapped particles. Introduce, now, the following *ballooning* representation of the EPM mode structure

$$\frac{e_H}{T_H} \delta\phi_k = e^{in\phi} \sum_m e^{-im\theta} \left(\int_{-\infty}^{\infty} e^{-i(nq-m)\eta} \Phi_0(\eta, \theta_k) d\eta \right) \frac{A(r,t)}{\sqrt{2\pi}} \quad , \tag{5}$$

where η is the extended poloidal angle, $\theta_k = (-i/nq')\partial_r$ acting on the EPM envelope $A(r,t)$ and $\Phi_0(\eta, \theta_k)$ is the ballooning EPM eigenfunction with the same normalizations chosen in Ref. [7]; *i.e.*, its large $|\eta|$ behavior can be written as

$$\Phi_0(\eta, \theta_k) = \frac{\left[a^{(\pm)} \cos(\eta/2) + b^{(\pm)} \sin(\eta/2) \right]}{\left\{ 1 + \left[s(\eta - \theta_k) - \alpha \sin\eta \right]^2 \right\}^{1/2}} \exp\left[-\epsilon_0 (\omega^2/\omega_A^2) a^{(\pm)} b^{(\pm)} \eta \right] \quad . \tag{6}$$

Here, $a^{(\pm)} = \sqrt{1 - \epsilon_0^{-1}[1 - \omega_A^2/(4\omega^2)]}$, $b^{(\pm)} = \pm\sqrt{1 + \epsilon_0^{-1}[1 - \omega_A^2/(4\omega^2)]}$, $(\pm)$ stands for (positive/negative) η, $\epsilon_0 = 2(\epsilon + \Delta')$, Δ' is the radial derivative of the Shafranov shift and $\omega_A = v_A/(qR_0)$ is the local value of the Alfvén frequency. Then, the linear energetic particle response in the ballooning representation is

$$\overline{\delta H}_k \simeq -\left(\frac{e}{m} \right) J_0(\gamma) \frac{QF_0}{\omega} \left[\Phi_0(\eta, \theta_k) - e^{-iQ_k} J_0(Q_{k0}) \frac{\bar{\omega}_d}{\bar{\omega}_d - \omega} \Phi_{0c}(\eta, \theta_k) \right] \quad , \tag{7}$$

where Q_k stands for Q_z with k_z substituted by k_r and with θ dependencies mapped into η, Q_{k0} is Q_k computed at $\theta = 0$ and $\Phi_{0c}(\eta, \theta_k)$ is $\Phi_0(\eta, \theta_k)$ with only $\propto \cos(\eta/2)$ dependencies included. Note that, here, we have assumed that finite banana width effects are dominated by geodesic curvature for finite magnetic shear [7]. Substituting back this expression into Eq. (4), we are still left with residual fast radial dependencies on the k_r^{-1} scale. In the present case, we are interested in nonlinear energetic particle distortions to the equilibrium fast ion pressure gradient on the k_z^{-1} scale, ordered as the EPM radial envelope width. We can, thus, further average Eq. (4) on the fast radial scale and we finally obtain

$$\frac{\partial}{\partial t} h_z = 2k_\theta^2 \rho_H^2 \frac{\omega_{cH}}{k_\theta} \frac{T_H}{m_H} \frac{\partial}{\partial r} \left[\mathbb{I}\mathrm{m} \left(\frac{QF_0}{\omega} \frac{\bar{\omega}_d}{\bar{\omega}_d - \omega} \right) \Gamma^2 \left| A \right|^2 \right]_H \quad . \tag{8}$$

Here, h_z is the spatially averaged expression of H_z, ρ_H is the energetic ion Larmor radius and T_H is the fast ion thermal energy. Furthermore, with $\gamma = k_\theta (1 + s^2\eta^2)^{1/2} (2\mu B_0)^{1/2} / \omega_c$, $Q_{k0} = k_\theta \theta_b s \eta q (v^2/2\epsilon)^{1/2} / \omega_c$ and θ_b the bounce angle,

$$\Gamma^2 = \int_{-\infty}^{\infty} J_0^2(\gamma) J_0^2(Q_{k0}) \left| \Phi_{0c}(\eta, \theta_k) \right|^2 d\eta \tag{9}$$

describes finite Larmor radius as well as banana width effects. Here, finite orbit width effects due to k_z are neglected since $|k_z| \ll |k_r|$.

The EPM dispersion relation, can be always expressed in the form [7]

$$\left[D_R(\omega,\theta_k;s,\alpha)+iD_I(\omega,\theta_k;s,\alpha)\right]A_0=\delta W_{KT}A_0 \quad , \tag{10}$$

where we have extracted the rapid EPM oscillation frequency from the mode amplitude as $A(r,t) = A_0(r,t)\exp(-i\omega_0 t)$, with $A_0(r,t)$ accounting for slow time variations only, *i.e.* $|\omega^{-1}\partial_t \ln A_0| \ll 1$. In Eq. (10), $\omega = \omega_0 + i\partial_t$ and $\theta_k = (-i/nq')\partial_r$ are operators acting on $A_0(r,t)$, and both real, D_R, and imaginary part, D_I, of the dispersion function can be formally treated as the principal symbol of a pseudo-differential operator [7, 23]. Furthermore, δW_{KT} is related to the fast ion contribution to the potential energy and can be written as [7]

$$\delta W_{K,T} = \frac{2\pi^2 e^2}{mc^2} qR_0B_0 \sum_{v_\parallel/|v_\parallel|=\pm}\int d\left(\frac{v^2}{2}\right)\int d\mu \frac{\bar\omega_d^2}{k_\theta^2}\tau_B\frac{QF_0}{\bar\omega_d-\omega} \quad , \tag{11}$$

where $\tau_B = 2\pi/\omega_B = 2\pi qR_0(2/v^2\epsilon)^{1/2}$ is the bounce period of deeply trapped ions. Note that Eq. (11) does not depend on the mode number, consistently with $s \approx 1$ and with the wavelength ordering $k_\theta\rho_H \lesssim \epsilon \lesssim k_\theta\rho_{BH} \lesssim \epsilon^{1/2} < 1$, assumed here, and corresponding to the most unstable conditions (ρ_{BH} is the fast ion banana width). Nonlinearly

$$QF_0 \to QF_0 + \frac{k_\theta}{\omega_c}\frac{\partial}{\partial r}h_z \quad , \tag{12}$$

and the EPM dispersion relation, Eq. (10), is readily generalized. To explicitly compute Eq. (11), we choose an isotropic slowing down distribution function, which has a cut-off at the fusion energy E_{fus} and is normalized to the fast alpha particle pressure P_H considering $E_{fus} \gg E_c$, with E_c the critical energy [24]: $F_0 = (3P_H)/(4\pi E_{fus})(v^3+(2E_c/m_H)^{3/2})^{-1}$. In this way, defining $\bar\omega_{dF}$ as $\bar\omega_d$ computed at E_{fus}, we obtain

$$\begin{aligned}\delta W_{K,T} = {} & \frac{3\pi\epsilon^{1/2}}{4\sqrt{2}}\alpha_H\left[1+\frac{\omega}{\bar\omega_{dF}}\ln\left(\frac{\bar\omega_{dF}}{\omega}-1\right)+i\pi\frac{\omega}{\bar\omega_{dF}}\right. \\ & \left. +i\pi\frac{\omega}{\bar\omega_{dF}}k_\theta^2\rho_H^2\frac{T_H}{m_H}\frac{1}{\alpha_H A_0}\partial_t^{-1}A_0\partial_r^2\partial_t^{-1}\left(\alpha_H|A_0|^2\right)\right] \quad .\end{aligned} \tag{13}$$

Here, ∂_t^{-1} is the standard notation for the inverse of ∂_t and we have kept the nonlinear modification to the imaginary part of $\delta W_{K,T}$ only, consistently with the ordering $|\omega^{-1}\partial_t| \ll 1$. Furthermore, we have assumed that the nonlinear time scale is sufficiently long to avoid destroying resonant wave-particle interactions. Substituting back into Eq. (10), we finally obtain

$$\begin{aligned}\left[D_R(\omega,\theta_k;s,\alpha)+iD_I(\omega,\theta_k;s,\alpha)\right]\partial_t A_0 = {} & \frac{3\pi\epsilon^{1/2}}{4\sqrt{2}}\alpha_H\left[1+\frac{\omega}{\bar\omega_{dF}}\ln\left(\frac{\bar\omega_{dF}}{\omega}-1\right)\right. \\ & \left. +i\pi\frac{\omega}{\bar\omega_{dF}}\right]\partial_t A_0 + i\pi\frac{\omega}{\bar\omega_{dF}}A_0\frac{3\pi\epsilon^{1/2}}{4\sqrt{2}}k_\theta^2\rho_H^2\frac{T_H}{m_H}\partial_r^2\partial_t^{-1}\left(\alpha_H|A_0|^2\right) \quad .\end{aligned} \tag{14}$$

Equation (14) can be taken as the starting point for detailed analyses of avalanche dynamics induced by EPM, which will be reported elsewhere. In the next Section, we present a discussion of Eq. (14) in the *local limit* and compare our findings with results from numerical simulations.

3. Discussions and Conclusions

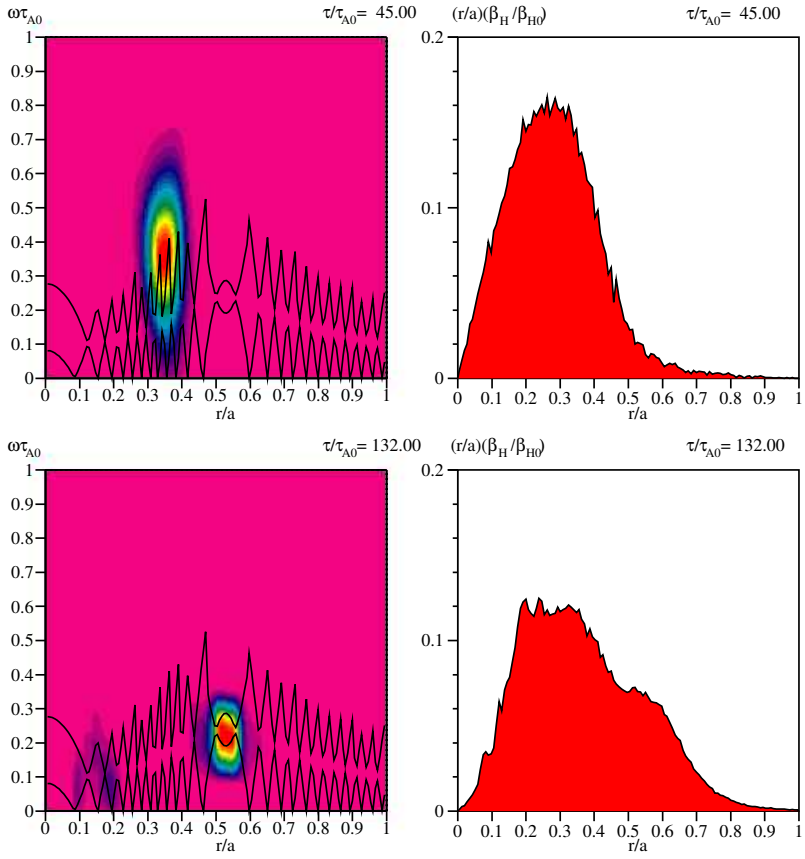

FIG. 2. Linearly unstable (top) and saturated (bottom) phases for on axis $\beta_{H0} = 0.025$ and the other profiles as discussed in Ref. [2, 20].

Consider again the case of Fig. 1, referring to a JET-like q-profile in reversed shear experiments with Alfvén Cascade excitation [4] and a model Maxwellian fast ion distribution function [2, 20]. Figure 2 shows the EPM intensity contour plots (left frames) and the corresponding fast ion surface density (right frames) for the linearly unstable and saturated phases of the EPM avalanche. The s.A. continuum is emphasized in black in the background of contour plots, with the visible effect of the minimum-q surface at $r/a \simeq 0.53$. Despite the difference in the fast ion sources – isotropic Maxwellian vs. the isotropic slowing down assumed here – we use Figs. 1 and 2 as a typical paradigm for EPM avalanches due to trapped energetic ions; *i.e.* the case for which, under simplifying assumptions, Eq. (14) was derived. Specifically, it can be shown that the $n = 4$ mode in Fig. 1 is driven mainly by the precession resonance ($\omega \simeq \bar{\omega}_d \propto nq$) at the radial position where the drive is strongest [11].

In order to investigate the nonlinear dynamics of EPM avalanches, it is instructive to solve Eq. (14) in the local limit. In fact, the narrow structure of the EPM envelope suggests to assume $|\theta_k| \ll 1$. Meanwhile, we can also consider that – near the peak of fast particle drive at r_0 – radial dependencies of the dispersion function are mainly due to the fast ion source profile, $\alpha_H = \alpha_{H0} \exp(-x^2/L_p^2)$, with $x = (r - r_0)$ and L_p the characteristic α_H scale length. Finally q profile changes account for the dominant radial variation of the s.A. continuum and $\bar{\omega}_{dF}$. In the linear limit, the mode frequency is determined by balancing D_R with $\mathbb{R}\mathrm{e}\delta W_{KT}$:

$$D_R(\omega_0, \theta_k = 0, s, \alpha) = \mathbb{R}\mathrm{e}\delta W_{KT}\big|_{x=0,\omega_0} \quad . \tag{15}$$

Meanwhile, the mode growth rate, γ_L is given by the competition between energetic particle drive $\propto \mathbb{I}\mathrm{m}\delta W_{KT}\big|_{x=0,\omega_0}$ and continuum damping $\propto D_I(\omega_0, \theta_k = 0, s, \alpha)$:

$$\gamma_L = \left(\mathbb{I}\mathrm{m}\delta W_{KT} - D_I\right) \left[\partial_{\omega_0} \left(D_R - \mathbb{R}\mathrm{e}\delta W_{KT}\right)\right]^{-1}\Big|_{x=0,\omega_0} \quad . \tag{16}$$

The radial dispersiveness, $\propto \theta_k^2$, balancing the energetic ion profile effects, $\propto \Big(\exp(-x^2/L_p^2) - 1\Big) \simeq -x^2/L_p^2$, finally gives a typical radial envelope width $\Delta \approx (L_p/k_\theta)^{1/2}$ and a complex frequency shift of $O(k_\theta^{-1} L_p^{-1})$ [8]. Nonlinearly, Eq. (14) shows that the EPM reduces the drive where the envelope is maximal and, at the same time, strengthens it in the nearby region, where $\partial_r^2 \ln |A|^2 > 0$. This behavior is clearly visible in the lower frames of Fig. 1. In order to maximize the drive, one readily sees that the EPM changes its radial localization according to

$$(x_0/L_p) = \gamma_L^{-1} k_\theta \rho_H \, (T_H/M_H)^{1/2} \, (|A_0|/W_0) \quad , \tag{17}$$

x_0 being the radial position of the maximum EPM amplitude, W_0 indicating the typical EPM radial width in the nonlinear regime and having used γ_L^{-1} to estimate the characteristic time in the early nonlinear phase. This displacement is clearly an avalanche, since the mode moves radially following an unstable propagating front. Note that the secular motion scales linearly with the mode amplitude, consistently with the numerical simulation in Fig. 1, and it is directed outwards since continuum damping is a decreasing function of (r/a) up to the minimum-q surface and then increasing again, as it is evident from Fig. 2. This fact clearly facilitates the secular motion up to the minimum-q surface, since the decreasing continuum damping partially compensates the weakening of the drive due to the local phenomena discussed in Sec. 1. Furthermore, this analysis provides an explanation of the reason why the EPM exhibits the natural tendency to merge into a Cascade mode at the minimum-q surface at the end of the convective amplification. Meanwhile, the real mode frequency still satisfies Eq.(15) computed at x_0. Therefore, the nonlinear frequency shift during the avalanche phase is

$$\Delta\omega = s \, \bar{\omega}_{dF}|_{x_0} \, (x_0/r) \, (\omega_0 / \, \bar{\omega}_{dF}|_{x=0}) \quad . \tag{18}$$

A posteriori, we may estimate the strength of EPM drive required to trigger an avalanche by the value, $\bar{x}_0$, of the convective displacement, given by Eq. (17), at the time the mode amplitude reaches the critical saturation value via wave-particle trapping, *i.e.* $\omega_b \approx \gamma_L$ [12, 13, 18], with the wave-particle trapping frequency ω_b such that $\omega_b^2 \approx k_\theta^2 \rho_H^2 k_\theta (T_H/m_H) R_0^{-1} |A|$ [12]. We readily obtain $\bar{x}_0 \approx R_0 \gamma_L / (k_\theta \rho_H)(T_H/m_H)^{-1/2} (\Delta^2/W_0)$. We can reasonably assume that the avalanching process is triggered when the EPM secular motion shifts its localization by one mode rational surface by the time wave-particle trapping becomes important. Meanwhile, the avalanching process is expected to become increasingly strong when the EPM secular displacement reaches up to a typical global mode width. Thus, in the very early nonlinear phase, we may expect that a weak avalanche is triggered when $k_\theta \bar{x}_0 \gtrsim 1$, *i.e.*

$$1 \gg \frac{\gamma_L}{k_\theta \rho_H (T_H/m_H)^{1/2} R_0^{-1}} \gtrsim (k_\theta L_p)^{-1/2} \quad , \tag{19}$$

while strong avalanching is expected to occur for $\bar{x}_0 \gtrsim W_0$, *i.e.*

$$1 \gg \frac{\gamma_L}{k_\theta \rho_H (T_H/m_H)^{1/2} R_0^{-1}} \gtrsim W_0^2/\Delta^2 \quad . \tag{20}$$

Note that $W_0^2/\Delta^2 \ll 1$ in Eq. (20) due to the short scale of the nonlinear distortion, $\delta\alpha_H$, in the equilibrium α_H profile, as it emerges from Fig. 1. Both Eqs. (19) and (20) show that the onset for EPM induced avalanches is close to the linear excitation threshold. If neither of these conditions is satisfied, EPM will saturate either via wave-particle trapping or other local phenomena, discussed in Sec. 1.

The relevance of strong energetic particle transport due to EPM convective amplification in burning plasmas is discussed in Ref. [11]. Meanwhile, experimental observations of rapid and macroscopic fast particle transports, like those associated with ALE on JT-60U [6], suggest that it is possible to excite large amplitude Alfvénic modes with signatures similar to EPMs. More recently, it has been shown that there exist Alfvénic fluctuations, characterized by rapidly chirping frequency, which are observed in JET in connection with excitation of large amplitude Alfvén Cascades [25, 26]. These fluctuations chirp downward in frequency and eventually merge into the spectral lines of Cascade modes, similarly to the qualitative behavior discussed above for EPM. It must be pointed out, though, that in the JET case precession-bounce resonances are more likely to play the dominant role. From our analysis, it is evident that an essential role in the avalanche dynamics is played by wave particle resonant interactions as well as by the s.A. continuous spectrum. Therefore, dedicated modeling is required for quantitative comparisons between theory, simulation and experiments.

[1] Chen, L., Phys. Plasmas **1** (1994) 1519.
[2] Zonca, F., Briguglio, S., Chen, L., Fogaccia, G., and Vlad, G., Paper TH/4-4. Presented at the 19.th IAEA Fusion Energy Conference, Lyon, France, Oct. 14-19, (2002).
[3] White, R.B., *et al.*, Phys. Fluids **26** (1983) 2958.
[4] Sharapov, S.E., *et al.*, Phys. Lett. A **289** (2001) 127.
[5] Zonca, F. , *et al.*, Phys. Plasmas **9** (2002) 4939.
[6] Shinohara, K., *et al.*, Nucl. Fusion **41** (2001) 603.
[7] Zonca, F., and Chen, L., Phys. Plasmas **3** (1996) 323.
[8] Zonca, F., and Chen, L., Phys. Plasmas **7** (2000) 4600.
[9] Zonca, F., Briguglio, S., Fogaccia, G., and Vlad, G., Presented at the 8th IAEA Technical Mtg. on Energetic Particles in Magnetic Conf. Systems, San Diego, CA, Oct 6–8 2003.
[10] Vlad, G., Briguglio, S., Fogaccia, G., and Zonca, F., *ibid.*.
[11] Vlad, G., *et al.*, *Effects of Alpha Particle Transport Driven by Alfvénic Instabilities on Proposed Burning Plasma Scenarios on ITER*, Presented at this Conference.
[12] Berk, H.L., and Breizman, B.N., Phys. Fluids B **2**, 2246, (1990).
[13] Berk, H.L., Breizman, B.N., and Pekker, M.S., Plasma Phys. Rep. **23** (1997) 778.
[14] Fasoli, A., *et al.*, Phys. Rev. Lett **81** (1998) 5564.
[15] Hahm, T.S., and Chen, L., Phys. Rev. Lett **74** (1995) 266.
[16] Zonca, F., Romanelli, F., Vlad, G., and Kar, C., Phys. Rev. Lett. **74** (1995) 698.
[17] Chen, L., *et al.*, Pl. Phys. Control. Fusion **40** (1998) 1823.
[18] Berk, H.L., Breizman, B.N., and Pekker, M.S., Phys. Rev. Lett **76** (1996) 1256.
[19] Zonca, F., Briguglio, S., Chen, L., Fogaccia, G., and Vlad, G., in *Theory of Fusion Plasmas*, pp. 17-30, J.W. Connor, O. Sauter and E. Sindoni (Eds.), SIF, Bologna, (2000).
[20] Briguglio, S., Vlad, G., Zonca, F., and Fogaccia, G., Phys. Lett. A **302** (2002) 308.
[21] Frieman, E.A., and Chen, L., Phys. Fluids **25** (1982) 502.
[22] Rosenbluth, M.N., and Hinton, F.L., Phys. Rev. Lett. **80** (1998) 724.
[23] Zonca, F., White, R.B., and Chen, L., Phys. Plasmas **11** (2004) 2488.
[24] Stix, T.H., Plasma Phys. **14** (1972) 367.
[25] Pinches, S.D., *et al.*, *The Role of Energetic Particles in Fusion Plasmas*, Presented at the 31st EPS Conf. on Plasma Physics, London June 28 – July 2nd (2004).
[26] Sharapov, S.E., *et al.*, *Experimental studies of instabilities and confinement of energetic particles on JET and on MAST*, Presented at this Conference.